Journal of Solid State Electrochemistry (2024) 28:3123–3132
https://doi.org/10.1007/s10008-024-05868-9

ORIGINAL PAPER

Electrochemical co-reduction of Mg(II), Al(III) and Nd(III) in the LiCl-NaCl-$MgCl_2$-AlF_3 melts

Mei Li[1] · Xuan Guo[1] · Yaochen Liu[1] · Rugeng Liu[1] · Meng Zhang[1] · Yang Sun[1] · Wei Han[1]

Received: 16 January 2024 / Revised: 19 March 2024 / Accepted: 21 March 2024 / Published online: 5 April 2024

Abstract

To prepare Mg–Al-Nd alloys electrochemically, the electrochemical co-reduction mechanism of Mg(II), Al(III), and Nd(III) was probed in the LiCl-NaCl-$MgCl_2$-AlF_3 melts on a molybdenum electrode by means of various electrochemical measurement techniques, i.e., cyclic voltammetry, square wave voltammetry, chronopotentiometry, and open circuit chronopotentiometry. It was found that Nd could deposit on pre-deposited Al metal and form Nd-Al intermetallics in the LiCl-NaCl-$NdCl_3$-$MgCl_2$-AlF_3 system, and the electrochemical signal related to the formation of ternary intermetallics was not detected. The co-reduction of Mg(II), Al(III), and Nd(III) was carried out on molybdenum electrode by galvanostatic electrolysis to prepare Mg–Al-Nd alloy, and samples were characterized by X-ray diffraction, scanning electron microscopy (SEM) with energy-dispersive spectrometry (EDS), and inductively coupled plasma-atomic emission spectrometry (ICP-AES). The results indicate that the alloy products were comprised of Al_2Nd intermetallic, Mg and Al phases, and the Mg–Al compound was not observed in the alloys.

Keywords Electrochemical co-reduction · Underpotential deposition · Mg–Al-Nd alloy · Galvanostatic electrolysis

Introduction

Mg–Al-based alloys are used extensively in many applications and fields due to their attractive properties, for instance, low density, strong corrosion resistance, high specific strength, and good stiffness [1, 2]. These Mg–Al family alloys have some limitations in engineering applications because the presence of $Mg_{17}Al_{12}$ phase is harmful to the mechanical properties of the alloys, such as tensile strength and creep resistance [3, 4]. In order to enhance the mechanical performance of Mg–Al alloys, many researchers explored the addition of other elements, such as Si, Ca, Ti, Gd, Y, and Zn, in Mg–Al alloys [5–12]. Among these researches, the Mg–Al-RE alloys have been paid special attention because the rare earth (RE) elements have been found to be very effective for improving the mechanical properties of Mg–Al based alloys at different temperatures. Adding small amounts of RE elements can have significant effects on the performance of magnesium alloys, since the RE elements may form stable intermetallic compounds with aluminum. Therefore, the Al-RE compounds are helpful for solution hardening and precipitation hardening in the alloys [13, 14].

The Mg–Al-RE alloys can be produced by mixing Mg, Al, and RE and vacuum melting in the laboratory or industry, while the molten salt electrolysis method may show more advantages in the metal production, such as the homogeneity of alloy composition, simplicity in technology, and continuous or semi-continuous manufacturing process [15]. So far, molten salt electrolysis is still the main method for industrial preparation of pure Mg, Al, and RE metals. More importantly, pure REs are extremely expensive because they are difficult to be extracted and purified. The preparations of Mg-RE and Al-RE alloys by molten salt electrolysis have been paid more attention in recent years. For example, the electrochemical formation of Mg-Pr [16, 17], Mg-Nd [18], Mg-Gd [19], Mg-Sm [20], Mg-Dy [21], Mg-Ho [22], Mg-Yb [23], Mg-Lu [24] alloys, and Mg-Li-RE (RE: Sm, La, Ce) alloys [25–27]. The aluminum alloys with rare earth elements such as Al-La [28], Al-Ce [29], Al-Sm [30], Al-Eu

✉ Yang Sun
sunyang@hrbeu.edu.cn

✉ Wei Han
weihan@hrbeu.edu.cn

[1] Key Laboratory of Superlight Materials and Surface Technology, Ministry of Education, College of Material Science and Chemical Engineering, Harbin Engineering University, Harbin 150001, China

[31, 32], Al-Tb [33], Al-Dy [34], Al-Er [35], and Al-Tm [36]. Al-Lu [37] and Al-Y [38] have also been prepared in different molten salts. As for the Mg–Al-RE alloys, Han et al. [39] studied the electrochemical formation of Mg–Al-Y alloy in the LiCl-NaCl-$MgCl_2$-AlF_3-YCl_3 system. They found that the underpotential depositions of Mg and Y on pre-deposited Al metal can lead to formation of Mg–Al and Al-Y alloy, and the existence of a certain amount of Y in the Mg–Al-Y alloy could restrain the formation of Mg–Al intermetallic compound. Jang et al. [40] probed the preparation of Mg–Al-La alloy in the KCl-$MgCl_2$-AlF_3-(La_2O_3) system. They reported that Mg–Al-La alloys with α-Mg, $Al_{11}La_3$, and β-$Al_{12}Mg_{17}$ phases were successfully obtained in the salt melts.

In this work, neodymium was chosen as the RE element because Nd has good affinity with Al and can form binary phases of Al_2Nd or $Al_{11}Nd_3$, which mainly distributed along the grain boundaries and can refine grain of Mg–Al alloy. The formation of Al-Nd binary phases can suppress the existence of the detrimental phase such as $Mg_{17}Al_{12}$ effectively, and improve tensile properties and corrosion resistance substantially for Mg–Al alloy [41, 42]. Thus, in order to prepare Mg–Al-Nd alloys, the co-reduction mechanism of Mg(II), Al(III), and Nd(III) ions was studied by employing a series of electrochemical techniques at 973 K (700 °C) in LiCl-NaCl-$MgCl_2$-AlF_3 molten salts. The alloy samples were obtained by galvanostatic electrolysis and analyzed by XRD and SEM–EDS.

Experimental

Salts preparation and purification

All the salts were firstly dried for more than 70 h at 573 K under high vacuum to remove residual moisture, and then LiCl, NaCl, and $MgCl_2$ (60:32:15 mass, analytical grade; Sinopharm Chemical Reagent Co. Ltd) were mixed and melted in a dry alumina crucible placed in an electric furnace. The melts temperature was measured by a nickel chromium-nickel aluminum thermocouple sheathed with an alumina tube. The pre-electrolysis was adopted at − 0.2 A (0.62 A/cm^2) and potential ranges from − 1.4 V to − 1.5 V (vs. $Ag|Ag^+$) for 1 h to get rid of impurities in the melts. All the operations were carried out in a glove box under argon atmosphere (less than 5 ppm O_2 and H_2O).

Experimental set-up

The electrochemical workstation (Autolab PGSTAT 302N, Metrohm, Ltd) controlled with the Nova 1.18 software was applied to electrochemical measurements. The transient electrochemical techniques were used to study the electrochemical behavior of Al(III), Mg(II), and Nd(III) in LiCl-NaCl melts. An electrochemical cell with three electrode set-up was employed. A silver wire (d = 1 mm) dipped into a solution of AgCl (0.1 wt%) in the LiCl-NaCl (3.0:1.6 mass) salts contained in an alundum tube was used as the reference electrode. All of the potentials were referred to this $Ag|Ag^+$ couple. The working electrode was molybdenum wire (d = 1 mm, 99.99% purity), which was contained in an alundum tube and polished entirely using SiC paper, and then cleaned ultrasonically in an ethanol bath. A spectrally pure graphite rod (d = 6 mm, 99.99% purity) in a quartz tube is adopted as the counter electrode. The surface area of reactive electrode was calculated by measuring the immersion depth of the electrode in the melts.

Characterization of products

The objective alloys were obtained by galvanostatic electrolysis with different conditions. After electrolysis, all the samples were washed in ethanol (99.9% purity) in an ultrasonic bath so as to eliminate adhered salts and preserved in a glove box for later analysis.

The prepared alloys were dissolved in HCl solution (5 wt%), and the content of Mg, Al, and Nd was determined using an inductively coupled plasma-atomic emission spectrometer (ICP-AES, IRIS Intrepid II XSP, Thermo Elemental). The microstructures and morphologies of the deposits were investigated by X-ray diffraction (XRD) (XPert Pro; Philips Co., Ltd) using Cu Kα radiation at 40 kV and 40 mA scanning electron microscopy (SEM) with energy-dispersive spectrometry (EDS) (JSM-6480A; JEOL Co., Ltd.)

Results and discussion

Electrochemical behavior of LiCl-NaCl-$NdCl_3$ salts

Figure 1 illustrates the cyclic voltammograms obtained at the Mo electrode in LiCl-NaCl melts in absence (dotted curve) and presence (solid curve) of $NdCl_3$ at 973 K. The peaks A/A′ (dotted line in Fig. 1) can be ascribed to the reduction/oxidation of M (M = Li and/or Na) on Mo electrode. After the addition of $NdCl_3$ into the melts, besides the anodic peak A′, the other two groups of oxidation peaks appear in solid curve, which implies that the reduction and oxidation of Nd(III)/Nd(0) is a two-step reaction. The peak C′ at about − 2.04 V are associated with the re-oxidation of Nd(III)/Nd(II) couple, and the peak B′ at approximately − 1.93 V should pertain to the re-oxidation of Nd(II)/Nd couple. The peaks B and C corresponding to the reduction of Nd(III) can be observed in the CV curve, but their exact location is difficult to be confirmed under the influence of the reductive peak of Li(I) or Na(I), so SWV was adopted in order to provide closer insight into electrochemical behavior of the LiCl-NaCl-$NdCl_3$ melts on Mo electrode.

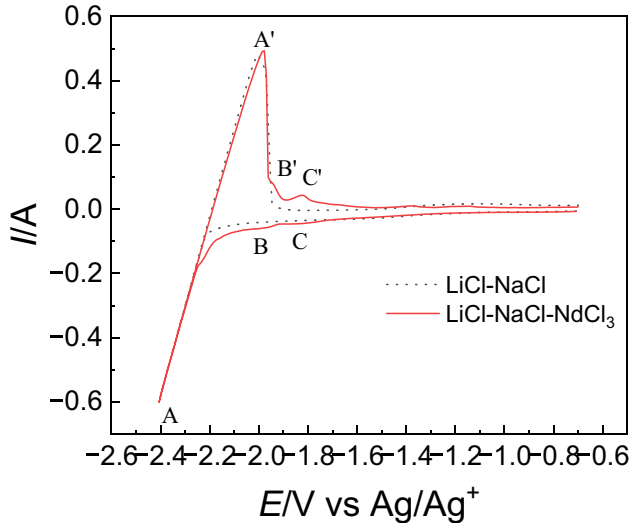

Fig. 1 Cyclic voltammograms obtained on Mo electrodes ($S=0.322$ cm^2) in the LiCl-NaCl eutectic melts before and after the addition of $NdCl_3$ (1.0 wt%) at 973 K; scan rate, 0.1 V s^{-1}.[1]

The square wave voltammetry is more sensitive than cyclic voltammograms and yield best peak resolution by potentials. Figure 2 shows a square wave voltammetry recorded at a step potential of 1 mV and frequency of 10 Hz plotted from − 1.0 V to − 2.3 V on Mo electrode at 973 K. It exhibits two obvious peaks B and C at − 2.04 V and − 1.98 V, corresponding to the reduction of Nd(II) and Nd(III), respectively. Thus, the electrochemical reductive process of Nd(III) in LiCl-NaCl-$NdCl_3$ (1.0 wt%) melts can be regarded as a two-step electron transfer mechanism, which can be summarized as follows:

$$Nd(III) + e^- \rightarrow Nd(II)$$

$$Nd(II) + 2e^- \rightarrow Nd(0)$$

As can be seen from Fig. 2, the SWV result is consistent with the one obtained from cyclic voltammograms in Fig. 1, and give more evident identification for the reductive peaks. The redox of Nd(III) has been confirmed as a two-step process in chloride melts according to prior studies, whereas there are some discrepancies for the descriptions of the electroreduction kinetics [43–47].

Figure 3 shows the cyclic voltammograms obtained in the LiCl-NaCl-$NdCl_3$ melts with different scan rates at 973 K. Five scan rates ranging from 100 to 500 mV s^{-1} were adopted in order to investigate the influence on the peak currents and potentials. From Fig. 3, it can be noticed that the peak potentials of Nd(II)/Nd are not constant but migrate to one direction with the change of sweep rate. Thus, the relationship between the peak potentials and the scan rate is analyzed and plotted as shown in Fig. 4, which indicates the cathodic peak potential (E_{pc}) and anodic peak potential (E_{pa}) of Nd(II) shift slightly towards the negative and positive direction, exhibiting a linear dependence with the logarithm of the scan rate. Thus, electrochemical redox of Nd(II)/Nd showed some irreversibility in LiCl-NaCl melts, and the results was in accordance with the previous works [45, 46], and this electrochemical behavior of Nd(II)/Nd was also verified and predicted by the model proposed by Akolkar et al. [48]. As for the transition of Nd(III) to Nd(II), the reduction process is generally considered as reversible in chloride eutectic mixture and corresponded to a more smooth peak in the CV curves [47–50].

Figure 5 presents the linear relationship between the reduction peak current of Nd(III) and the square root of the scan rate, indicating that the electrochemical reduction

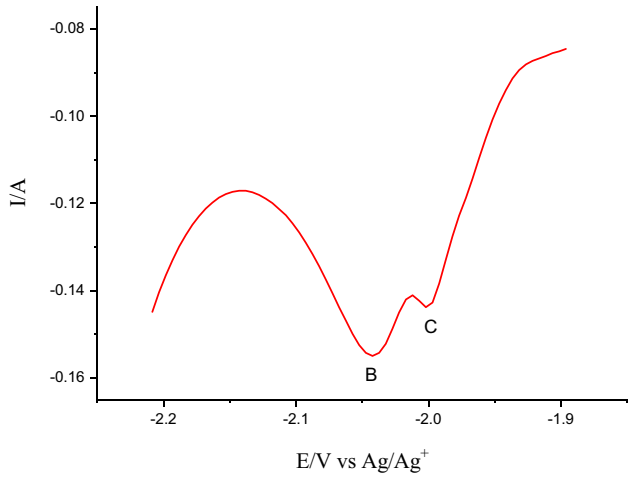

Fig. 2 Square wave voltammograms for the reduction of Nd on Mo electrode in the LiCl-NaCl-$NdCl_3$ (1.0 wt%) melts. Frequency, 10 Hz; T, 973 K

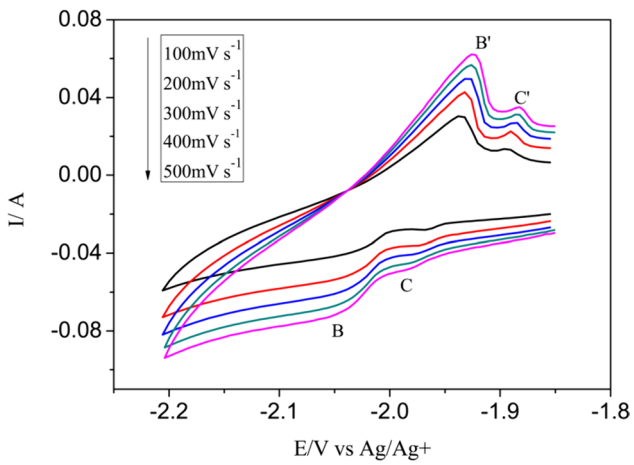

Fig. 3 Cyclic voltammogram obtained in the LiCl-NaCl-$NdCl_3$ (1.0 wt%) melts at different scan rates using a Mo ($S=0.322$ cm^2) electrode at 973 K

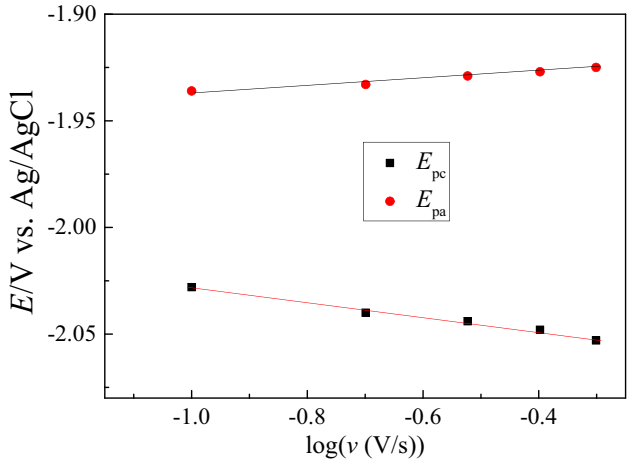

Fig. 4 The relationship between the cathodic and anodic peak potentials of Nd(II) with the logarithm of the scan rates in fused LiCl-NaCl-$NdCl_3$ at 973 K

process of Nd(III)/Nd(II) is diffusion-controlled at low scan rate for this soluble-soluble transition. Therefore, the Randles-Sevčik equation was applied to give an estimation of the diffusion coefficient for the reduction of Nd(III) in the LiCl-NaCl melts [51]:

$$I_p = 0.44AC_0(nF)^{3/2}(Dv/RT)^{1/2} \quad (1)$$

where A is the electrode surface area (cm^2), C_0 is the solute concentration (mol cm^{-3}), D is the diffusion coefficient (cm^2 s^{-1}), F is the Faraday constant (96,500 C mol^{-1}), R is the ideal gas constant (J K^{-1} mol^{-1}), n is the number of exchanged electrons, v is the potential sweep rate (V s^{-1}), and T is the absolute temperature (K).

According to the Randles-Sevčik equation, we can calculate the diffusion coefficient of Nd(III); the value of D is 2.38×10^{-5} cm^2 s^{-1}, which is close to the results obtained in the LiCl–KCl melts at lower temperature [52, 53].

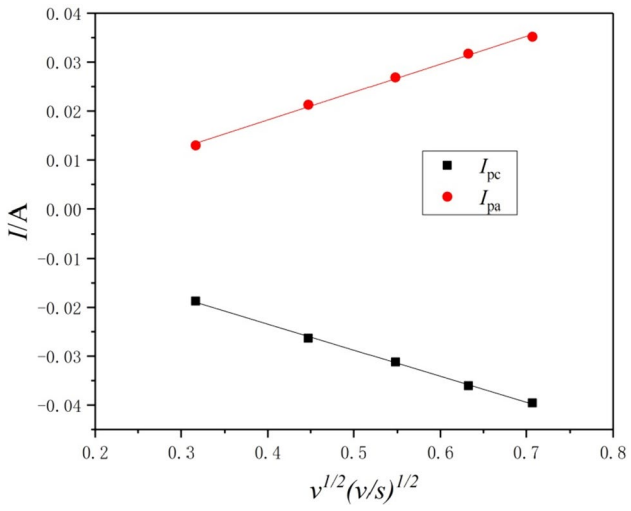

Fig. 5 Variation of the cathodic and anodic peak current of Nd(III) with the square root of the scan rate in fused LiCl-NaCl-$NdCl_3$ at 973 K

Electrochemical behavior of LiCl-NaCl-$NdCl_3$ salts in the presence of $MgCl_2$ and AlF_3

Figure 6 presents the cyclic voltammograms obtained on Mo electrode in the LiCl-NaCl salts at 973 K with the absence and presence of $MgCl_2$ and AlF_3, respectively. From the curve obtained in LiCl-NaCl-$MgCl_2$ in Fig. 6(a), except for the peaks A/A′ corresponding to the redox of M(I)/M (M = Li and/or Na), the new deposition/reoxidation peaks D/D′ observed at about − 1.76 V/ − 1.55 V can be ascribed to the formation of Mg and its oxidation. Signals E/E′ in Fig. 6(b) at approximately − 0.98 V/ − 0.76 V (vs. $Ag|Ag^+$) correspond to the reduction of Al(III) and re-oxidation of deposited Al.

In order to learn the comprehensive mechanism of the alloy formation, the cyclic voltammograms of three molten salt systems with different compositons were carried out as shown in Fig. 7. In the LiCl-NaCl-$MgCl_2$ (1.0 wt%)-AlF_3 (1.0 wt%) system (curve 1), three groups of cathodic/anodic signals (A/A′, D/D′, and E/E′) are related to the reduction and subsequent oxidation of M (M = Li and/or Na), Mg and Al, respectively. The reductive processes corresponding to peaks of D and E can be summarized as follows:

$$Mg(II) + 2e^- = Mg(0).$$

$$Al(III) + 3e^- = Al(0).$$

Curve 2 stands for the cyclic voltammograms of the LiCl-NaCl-AlF_3 (1.0 wt%)-$NdCl_3$ (1.0 wt%) system. Unlike curve 1, the signal for the redox of Al is less obvious due to the formation of intermetallic compounds. The new peaks of F′ and G′ should pertain to the re-oxidation of two Al-Nd intermetallic compounds, which were reduced by the under-potential deposition of Nd on the pre-deposition aluminum. The formation of Al-Nd compounds can be described as follows:

$$Nd(III) + 3e^- + xAl = AlxNd \quad (2)$$

Curve 3 displays the cyclic voltammograms of the LiCl-NaCl-$MgCl_2$-AlF_3-$NdCl_3$ system. Just as curve 2, the signals F′ and G′ are related to the re-oxidation of the deposited Al-Nd intermetallic compounds. The signal D/D′ standing for the reduction and oxidation of Mg(II) can still be observed in curve 3. However, the redox signals correlated

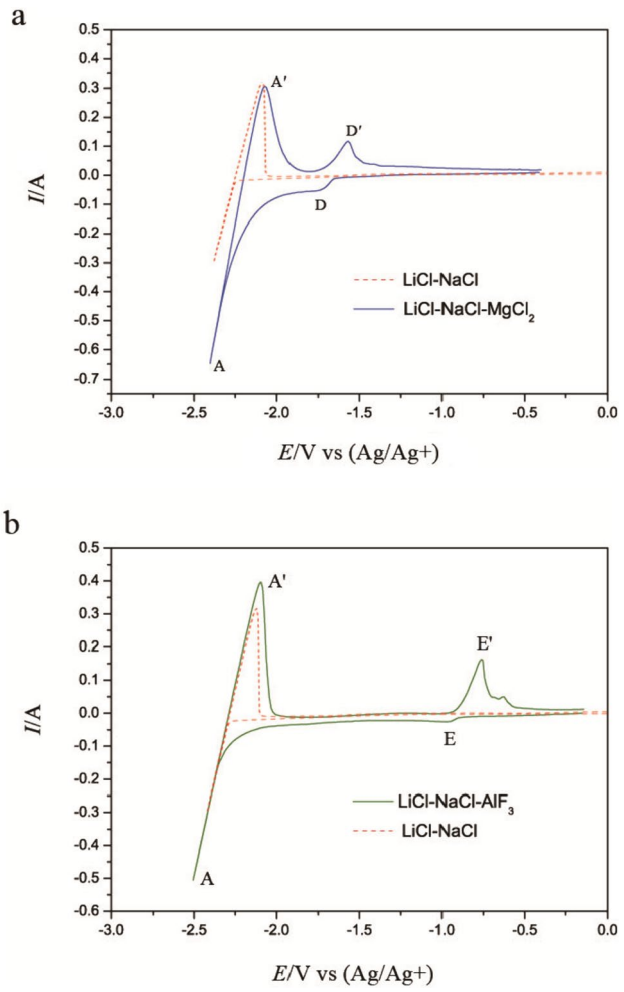

Fig. 6 The cyclic voltammograms obtained in the LiCl-NaCl salts before and after the addition of $MgCl_2$ (1.0 wt%) and AlF_3 (1.0 wt%) on a Mo electrode ($S = 0.322$ cm^2) at 973 K with a scan rate of 100 mV s$^{-.1}$

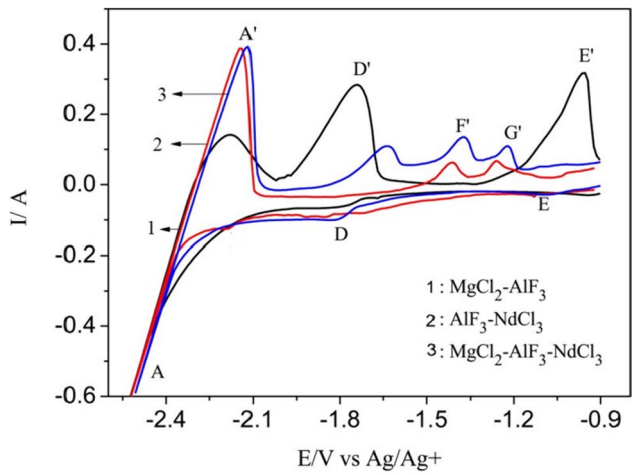

Fig. 7 The cyclic voltammograms of (1) LiCl-NaCl-$MgCl_2$-AlF_3; (2) LiCl-NaCl-AlF_3-$NdCl_3$; and (3) LiCl-NaCl-$MgCl_2$-AlF_3-$NdCl_3$ on a Mo electrode ($S = 0.322$ cm^2) at 973 K with a scan rate of 100 mV s.$^{-1}$

with the formation and oxidation of Mg-Nd and Mg–Al intermetallic compounds are not found.

In order to get more information for the electrochemical co-deposition of Mg–Al-Nd alloys, a group of chronopotentiometry measurements were carried out on Mo electrode ($S = 0.322$ cm^2) in the LiCl-NaCl-$MgCl_2$ (1.0 wt%)-AlF_3 (1.0 wt%)-$NdCl_3$ (1.0 wt%) molten salts as shown in Fig. 8. At a cathodic current of − 20 mA (− 0.062 A/cm^2), only a potential plateau E can be found, and it is corresponding to the deposition of aluminum. While the cathodic current reaches − 40 mA (− 0.124 A/cm^2), apart from the plateau E, the curve exhibits a new potential plateau F, which is related to the formation of an Al-Nd intermetallic compound. As the cathodic current increases from − 60 to − 100 mA, the curves show another new potential plateau D, which belongs to the deposition of magnesium. When the current exceeds − 140 mA (− 0.435 A/cm^2), a fourth plateau B associated with the formation of pure Nd metal reduced from Nd(II) can be observed. At this current density, electrochemical co-reduction of Mg, Al, and Nd occurs. The results are consistent with the potential range in the cyclic voltammograms Fig. 7.

Figure 9 shows the open circuit chronopotentiograms after galvanostatic electrolysis at − 2.3 V (vs. Ag|Ag$^+$) for 60 s in LiCl-NaCl-$MgCl_2$ (1.0 wt%)-AlF_3 (1.0 wt%)-$NdCl_3$ (1.0 wt%) melts at 973 K on Mo electrode. The composition of the electrode surface maintained a two-phase coexisting state with certain proportion during this process, and the corresponding potential plateau is observed in the curves [54]. It can be seen from Fig. 9 that there are six potential plateaus

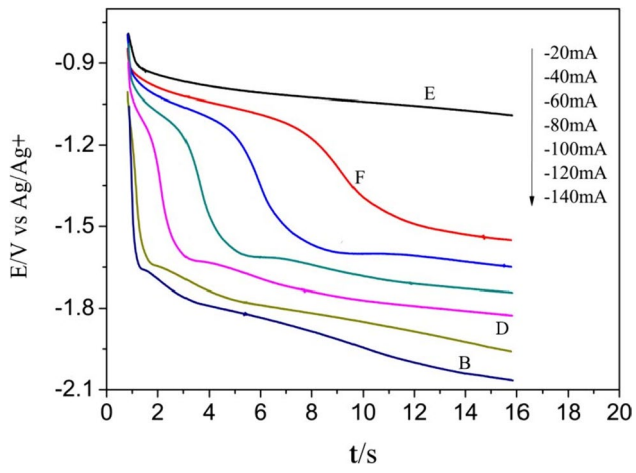

Fig. 8 The chronopotentiograms obtained from the LiCl-NaCl-$MgCl_2$ (1.0 wt%)-AlF_3 (1.0 wt%)-$NdCl_3$ (1.0 wt%) molten salts at different current intensities on a Mo electrode ($S = 0.322$ cm^2) at 973 K

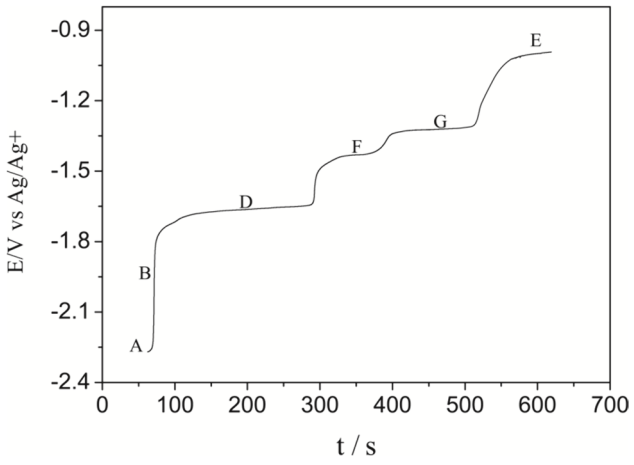

Fig. 9 The open circuit chronopotentiograms collected in the LiCl-NaCl-$MgCl_2$-AlF_3-$NdCl_3$ molten salts at 973 K on a Mo electrode ($S = 0.322$ cm^2) after galvanostatic electrolysis at − 2.30 V (vs. Ag/AgCl) for 700 s

that could be identified. First potential A at around − 2.16 V is related to the presence of deposited M metal (M = Li and/or Na) on the electrode. After plateau A, two potential plateaus B and D are observed at − 1.9 V and − 1.65 V, respectively. The plateaus B and D are related to the deposited Nd and Mg metal according to the cyclic voltammograms discussed above. The potential plateaus F and G (− 1.4 V and − 1.3 V) are interpreted as the equilibrium presence of Al-Nd intermetallic compounds, corresponding to the F′ and G′ peaks of the CV in Fig. 7. The last plateaus E at − 0.97 V pertained to the Al(III)/Al equilibrium potentials, as can also be observed by cyclic voltammograms.

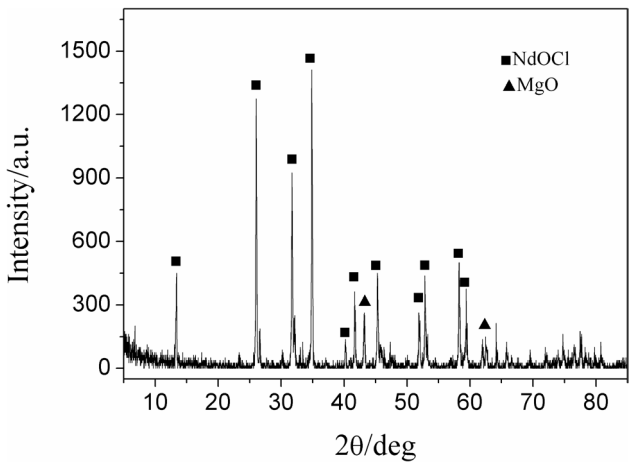

Fig. 10 XRD patterns of the bottom salts form LiCl-NaCl-$MgCl_2$-Nd_2O_3 melts after heating 1 h at 973 K

Galvanostatic electrolysis and characterization of the deposits

Based on the results of cyclic voltammetry, square wave voltammetry, chronopotentiometry, and open circuit chronopotentiometry, it was demonstrated that the preparation of Mg–Al-Nd alloys is feasible in molten salts by electrochemical methods, and galvanostatic electrolysis was adopted for the formation of the co-deposited products. As $NdCl_3$ has a series of disadvantages, Nd_2O_3 should play more important role in the future engineering production. Thus, Nd_2O_3 instead $NdCl_3$ is introduced in LiCl-NaCl-$MgCl_2$-AlF_3 melts. According to our previous experimental results [55], the rare earth oxides can be dissolved and chlorinated with the aid of $MgCl_2$ as the following reaction:

$$3MgCl_2(l) + RE_2O_3(s) = 3MgO(s) + 2RECl_3(l) \quad (3)$$

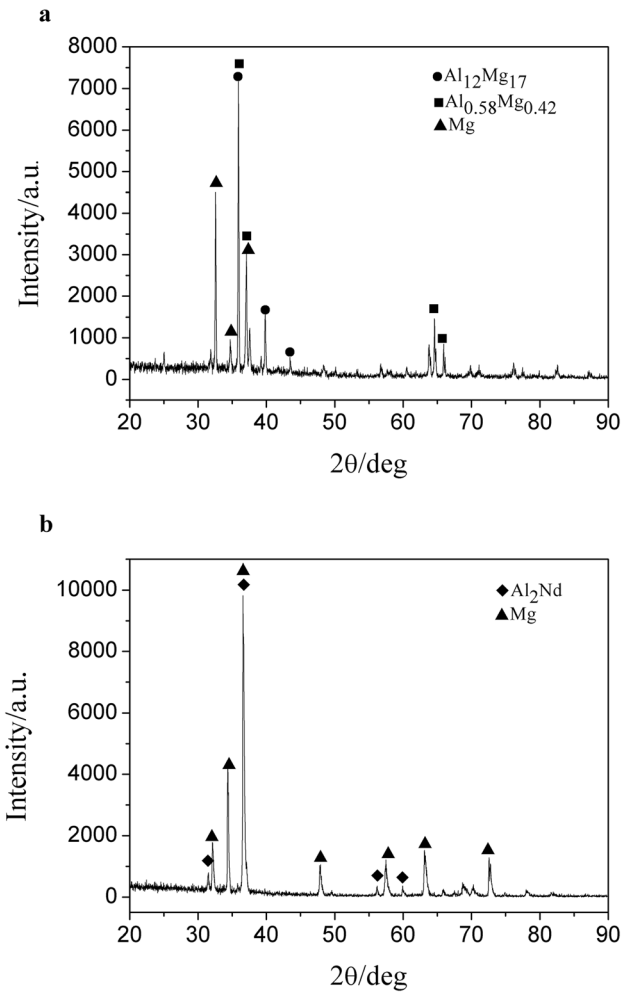

Fig. 11 XRD patterns of samples obtained by galvanostatic electrolysis on a Mo electrode ($S = 0.322$ cm^2) in the LiCl-NaCl-$MgCl_2$-AlF_3 salts before (a) and after (b) the addition of Nd_2O_3 for 3 h at 1023 K. Cathode-current density, 3.1 A/cm.^{2}

Figure 10 shows the XRD patterns of the bottom salts of the cooling LiCl-NaCl-$MgCl_2$-Nd_2O_3 melts (60 g: 32 g: 15 g: 5 g) after heating 1 h at 973 K in order to examine chlorination result of Nd_2O_3. It can be seen from Fig. 10 that the compositions of the sediments are mainly MgO and NdOCl, indicating Nd_2O_3 has been reacted with $MgCl_2$ at this temperature. The analysis of the ICP-AES also confirmed existence of Nd(III) in molten salts, so it can be deduced that the $MgCl_2$ can chlorinate Nd_2O_3 effectively for the successive electrolysis in the melts.

From chronopotentiograms in Fig. 9, the current density should be negative than -0.435 A/m^2 so as to obtain the co-reduction samples of alloy. Thus, the more negative current density was adopted for the galvanostatic electrolysis in the LiCl-NaCl-$MgCl_2$-AlF_3-Nd_2O_3 melt system under different conditions.

Figure 11 shows the XRD patterns of alloy sample obtained by galvanostatic electrolysis from the LiCl-NaCl-$MgCl_2$-AlF_3 molten salts before and after the addition of 0.35 wt% Nd_2O_3 with the current density 3.1 A/cm^2 at 1023 K. As can be seen from the XRD patterns, the alloys are composed of $Al_{12}Mg_{17}$, $Al_{0.58}Mg_{0.42}$, and Mg without the presence of Nd_2O_3. While after the Nd_2O_3 was added into the LiCl-NaCl-$MgCl_2$-AlF_3 salts, the Mg–Al phase disappears, and the samples are mainly composed of Al_2Nd and Mg phases, which indicates that the existence of a certain amount of Nd element in the Mg–Al-Nd alloy can inhibit the formation of Mg–Al compound, which could affect the mechanical performance of Mg–Al based alloys. The XRD patterns are also consistent with the results of the above electrochemical analysis.

Figure 12 presents the SEM microstructure analysis of the bulk alloy obtained by galvanostatic electrolysis from the LiCl-NaCl-$MgCl_2$-AlF_3-Nd_2O_3 melts at 1023 K. From the SEM, we can see that there are gray and bright grain-like zones. To confirm and examine the distributions of Mg, Al, and Nd elements in the alloy, a mapping analysis is employed as shown in Fig. 12. Mapping analysis indicates that Mg element mainly distributes in gray matrix zones, and Al element distributes homogeneously throughout gray zone and bright zones. The Nd element distribution is not uniform and disperse mainly within bright zones.

Figure 13 gives the EDS results of the points labeled A, B, and C taken from three represented zones which is displayed in Fig. 12. The EDS analysis indicates the atomic ratio of Al to Nd is about 4.12 in the point of A, which is chosen from bright zones. Just as shown in the mapping analysis, there is no Nd found in the point of B or C taken from gray zones, which consist of Mg and Al elements with certain percentage. The results indicate that the preparation of Mg–Al-Nd alloy by electrochemical co-reduction is feasible in the melts.

The current efficiency was calculated using the following equation in order to obtain the most suitable conditions for galvanostatic electrolysis [20]:

$$\eta = (Q_{Mg} + Q_{Al} + Q_{Nd})/It \quad (4)$$

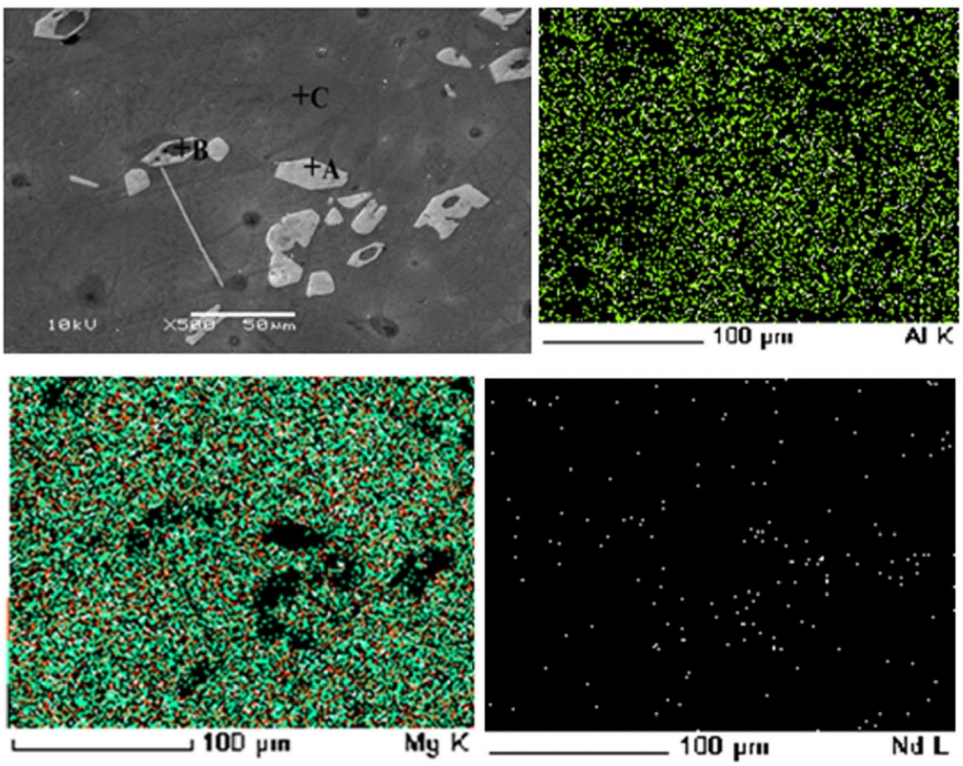

Fig. 12 The SEM image and EDS mapping analysis of alloy obtained by galvanostatic electrolysis in the LiCl-NaCl-$MgCl_2$-AlF_3-Nd_2O_3 molten salts on a Mo electrode ($S = 0.322$ cm^2) at 3.1 A/cm^2 for 3 h at 1023 K

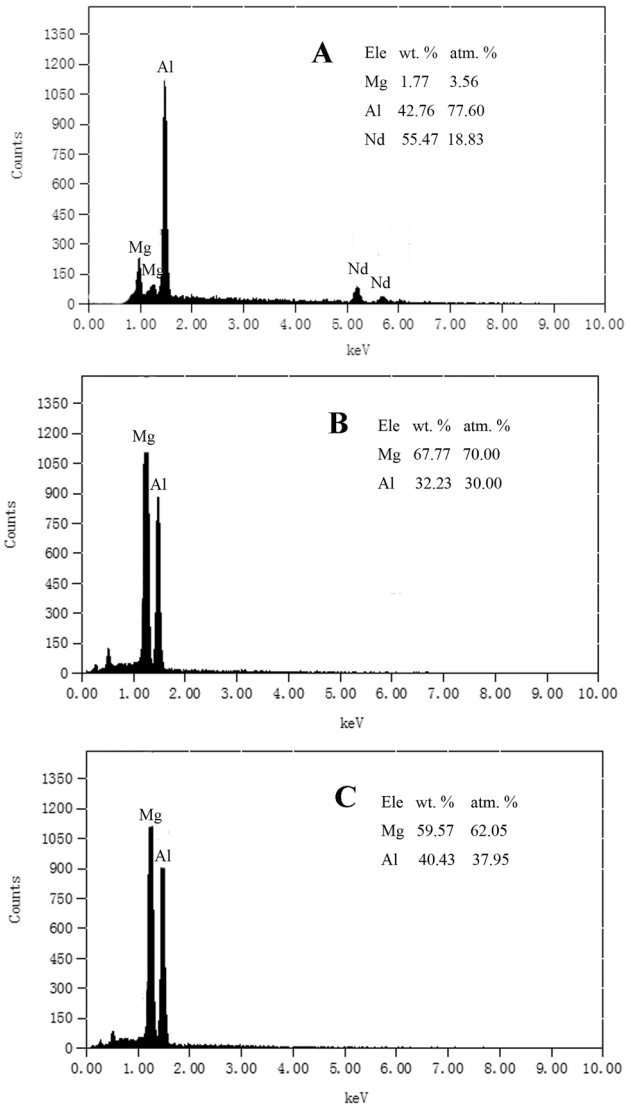

Fig. 13 EDS analysis for chemical constitutions of points A, B, and C as shown in Fig. 12

where Q_{Mg}, Q_{Al}, and Q_{Nd} are the charges of the deposited Mg, Al, and Nd, respectively, A·h; t is the electrolysis time, h; and I is the current intensity, A.

According to Faraday's law:

$$Q = nzF \tag{5}$$

where n is the amount of metal material deposited, mol; z is the number of electrons transferred in the reaction; and F is the Faraday constant, 26.801 A h mol^{-1}.

Galvanostatic electrolysis was conducted under different conditions to get the optimal parameters for the alloy yield or current efficiency. The alloy samples were dissolved and analyzed by ICP-AES, and the influence of the temperature, current density, and electrolysis time was considered.

Table 1 The ICP-AES analysis of some samples obtained in LiCl-NaCl-$MgCl_2$-AlF_3-Nd_2O_3 molten salts by galvanostatic electrolysis at different conditions

No	$MgCl_2$ (g)	AlF_3 (g)	Nd_2O_3 (g)	I (A)	T (°C)	Mg (%)	Al (%)	Nd (%)	Time (h)	Current efficiency (%)
1	10	10	0.5	1.0	650	91.9	4.5	3.6	1.0	49.0
2	15	10	0.5	1.0	700	84.1	9.1	6.8	2.5	65.8
3	15	9	0.6	3.0	750	78.2	13.5	8.3	1.5	73.5
4	15	8	1.0	1.0	800	71.5	17.2	11.3	3.0	68.5
5	15	5	0.5	2.0	700	85.1	9.8	5.1	3.0	63.8
6	14	6	0.8	4.0	750	72.5	16.4	11.1	2.0	68.4
7	13	7	0.4	2.0	700	87.6	8.3	4.1	3.0	62.3

The results indicate the current efficiency was increased with the increase of the temperature until 750 °C (1023 K), when the other conditions remain constant. The current efficiency increased rapidly with the extension of electrolysis time, while it would descend when the time were longer than 1.5 h. The enhancement of the current density can also lead to the increase of the current efficiency; the maximum value for the current density is at around 0.932 A/cm^2. As for the composition of the alloy samples, it was shown that the content of Mg among the alloy decreased and the content of Al and Nd increased continuously with the raise of temperature, current density, and electrolysis time. Furthermore, we can notice that the content of the Nd among the alloy samples increased with the addition of Nd_2O_3 in the melts.

Some typical conditions and results are listed in Table 1. The current efficiency was higher than 60% in most cases, and it has the maximum value of 73.5% at the temperature of 1023 K (750 °C) and 9.32 A/cm^2 for 1.5 h. The difficulties for the increasement of current efficiency should be ascribe to the multivalency of Nd species, i.e., the redox shuttling between Nd(II) and Nd(III), or disproportionation reaction such as $Nd(metal) + Nd(III) \rightleftharpoons 2Nd(II)$ [45, 56, 57]. Therefore, the yield for the Mg–Al-Nd alloys still has potentials to be enhanced if the multivalent behavior of Nd is well controlled with appropriate conditions.

Conclusion

The electrochemical behaviors of Nd(III) ions and the preparation mechanism of Mg–Al-Nd alloys by co-reduction were studied in LiCl-NaCl-$MgCl_2$-AlF_3 melts with different techniques on the molybdenum electrode. The results indicate that Nd(III) ions were reduced to Nd by two-step of electron transfer process in LiCl-NaCl-$NdCl_3$ melts at 973 K, while the addition of Nd(III) can lead to Nd-Al intermetallic phase in the LiCl-NaCl-$MgCl_2$-AlF_3 system with the same conditions. The co-reduction of Mg–Al-Nd alloys was prepared by galvanostatic electrolysis according to the electrochemical results, and the alloy samples were characterized by XRD, SEM, and ICP-AES. The prepared alloy was comprised of intermetallic compound Al_2Nd, Mg and Al phase, and the Mg–Al intermetallic compound that may be detrimental to the alloys were not observed. The composition of alloy was consistent with results of electrochemical studies. The current efficiency could reach 73.5% at 9.32 A/cm^2 for 1.5 h from the results of ICP-AES.

Funding The work was financially supported by the National Natural Science Foundation of China (U2167215, 22076035, 11875116, and 21876034) and the Fundamental Research Funds for the Central Universities (3072022JC1501).

References

1. Mordike BL, Ebert T (2001) Magnesium-properties-application-potential. Mater Sci EngA 302:37–45
2. Gray J, Luan B (2002) Protective coatings on magnesium and its alloys-a critical review. J Alloy Compd 336:88–133
3. Kleiner S, Beffort O, Wahlen A, Uggowitzer PJ (2002) Microstructure and mechanical properties of squeeze cast and semi-solid cast Mg-Al alloys. J Light Met 2:277–280
4. Kurnaz SC, Sevik H, Açıkgöz S, Özel A (2011) Influence of titanium and chromium addition on the microstructure and mechanical properties of squeeze cast Mg-6Al alloy. J Alloy Compd 509:3190–3196
5. Lee YC, Dahle AK, StJohn DH, Hutt JEC (1999) The effect of grain refinement and silicon content on grain formation in hypoeutectic Al-Si alloys. Mater Sci Eng A 259:43–52
6. Shaw C, Jones H (1999) Structure and mechanical properties of two Mg-Al-Ca alloys consolidated from atomized power. Mater Sci Tech 15:78–83
7. Li SS, Tang B, Zeng DB (2007) Effects and mechanism of Ca on refinement of AZ91D alloy. J Alloys Compd 437:317–321
8. Prasad YVRK, Rao KP, Hort N, Kainer KU (2009) Optimum parameters and rate-controlling mechanisms for hot working of extruded Mg-3Sn-1Ca alloy. Mater Sci Eng A 502:25–31
9. Gao L, Chen RS, Han EH (2009) Effects of rare-earth elements Gd and Y on the solid solution strengthening of Mg alloys.J Alloys Compd 481:397–394
10. Rokhlin LL, Nikitina NI (1998) Recovery after ageing of Mg-Y and Mg-Gd alloys. J Alloys Compd 279:166–170
11. Wang J, Meng J, Zhang DP, Tang DX (2007) Effect of Y for enhanced agehardening response and mechanical properties of Mg-Gd-Y-Zr alloys. Mater Sci Eng A 456:78–84
12. Liu XB, Chen RS, Han EH (2008) Effects of ageing treatment on microstructures and properties of Mg-Gd-Y-Zr alloys with and without Zn additions. J Alloys Compd 465:232–238
13. Yuan W, Liang Z, Zhang C (2012) Effects of La addition on the mechanical propertiesand thermal-resistant properties of Mg-Al-Si-Zr alloys based on AA 6201. Mater Des 34:788–792
14. Zhou WW, Cai B, Li W (2012) Heat-resistant Al-0.2Sc-0.04Zr electrical conductor. Mater Sci Eng A 552:353–358
15. Han W, Li M, Zhang ML, Yan YD (2016) Progress in preparation of rare earth metals andalloys by electrodeposition in molten salts. Rare Met 35:811–825
16. Tang H, Yan YD, Zhang ML, Li X, Han W, Xue Y, Zhang ZJ, He H (2013) Fabrication of Mg-Pr and Mg-Li-Pr alloys by electrochemical co-reduction from their molten chloride. Electrochim Acta 107:209–215
17. Wang YC, Li M, Han W, Zhang ML, Yang YS, Sun Y, Zhao YC, Yan YD (2015) Electrochemical extraction and separation of praseodymium and erbium on reactive magnesium electrode in molten salts. J Solid State Electrochem 19(12):3629–3638
18. Fu YZ, Zhang ZM, Lu XC, Pan BF, Zhang LP (2022) Preparation of Mg-Nd alloys by magnesiothermic reduction in molten salt. Metall Mater Trans B 53(1):617–626
19. Yang YS, Zhang ML, Han W, Sun PY, Liu B, Jiang HL, Jiang T, Peng SM, Li M, Ye K, Yan YD (2014) Selective electrodeposition of dysprosium in LiCl-KCl-$GdCl_3$-$DyCl_3$ melts at magnesium electrodes: application to separation of nuclear wastes. Electrochim Acta 118:150–156
20. Yang YS, Zhang ML, Han W, Jiang HL, Li M, Ye K, Yan YD (2014) Selective extraction of gadolinium from Sm_2O_3 and Gd_2O_3 mixtures in a single step assisted by $MgCl_2$ in LiCl-KCl melts. J Solid State Electrochem 18(3):843–850

21. Zhang ML, Yang YS, Han W, Li M, Sun Y, Yan YD (2013) Separation of $SmCl_3$ from $SmCl_3$-$DyCl_3$ system by electrolysis in KCl-LiCl-$MgCl_2$ molten salts. Energy Procedia 39:375–381
22. Wang J, Li M, Han W, Liu ZY, Yang XG, Sun Y, Zhang ML (2022) Electrochemical co-reduction of holmium and magnesium ions in eutectic LiCl-KCl salts. Rare Met 41(4):1394–1402
23. Chen Y, Ye K, Zhang ML (2010) Preparation of Mg-Yb alloy film by electrolysis in the molten LiCl-KCl-$YbCl_3$ system at low temperature. J Rare Earth 28(1):128–133
24. Jiang T, Wang N, Peng SM, Li M, Han W, Zhang ML (2015) Electrochemical formation of Mg-Lu alloy and alloy layer in molten LiCl-KCl. J Alloy Compd 658:198–209
25. Han W, Tian Y, Zhang ML, Ye K, Zhao QY, Wei SQ (2009) Preparation of Mg-Li-Sm alloys by electrocodeposition in molten salt. J Rare Earth 27:1046–1050
26. Zhang ML, Cao P, Han W, Yan YD, Chen LJ (2012) Preparation of Mg-Li-La alloys by electrolysis in molten salt. Trans Nonferrous Met Soc China 22:16–22
27. Zhang M, Han W, Zhang ML, Zhu FY, Xue Y, Zhang ZJ (2013) Electrochemical formation process and phase control of Mg-Li-Ce alloys in molten chlorides. J Rare Earth 31:609–615
28. Liu YL, Yuan LY, Ye GA, Liu K, Zhu L, Zhang ML, Chai ZF, Shi WQ (2014) Co-reduction behaviors of lanthanum and aluminium ions in LiCl-KCl eutectic. Electrochim Acta 147:104–113
29. Wang L, Liu YL, Liu K, Tan SL, Yan LY, Su LL, Chai ZF, Shi WQ (2014) Electrochemical extraction of cerium from CeO_2 assisted by $AlCl_3$ in molten LiCl-KCl. Electrochim Acta 147:385–391
30. Castrillejo Y, Fernández P, Medina J, Hernández P, Barrado E (2011) Electrochemical extraction of samarium from molten chlorides in pyrochemical processes. Electrochim Acta 56:8638–8644
31. Bermejo MR, Rosa F, Barrado E, Castrillejo Y (2007) Cathodic behaviour of europium (III) on glassy carbon, electrochemical formation of Al4Eu, and oxo acidity reactions in the eutectic LiCl-KCl. J Electroanal Chem 603(1):81–95
32. Bae SE, Park YJ, Min SK, Cho YH, Song K (2010) Aluminum assisted electrodeposition of europium in LiCl-KCl molten salt. Electrochim Acta 55(8):3022–3025
33. Li M, Gu QQ, Han W, Yan YD, Zhang ML, Sun Y, Shi WG (2015) Electrodeposition of Tb on Mo and Al electrodes: thermodynamic properties of $TbCl_3$ and $TbAl_2$ in the LiCl-KCl eutectic melts. Electrochim Acta 167:139–146
34. Su LL, Liu K, Liu YL, Wang L, Yuan LY, Wang L, Li ZJ, Zhao XL, Chai ZF, Shi WQ (2014) Electrochemical behaviors of Dy(III) and its co-reduction with Al(III) in molten LiC-KCl salts. Electrochim Acta 147:87–95
35. Sun Y, Zhang ML, Han W, Yan YD, Yang YS, Sun YX (2013) Electrochemical behaviour and codeposition of Al-Li-Er alloys in LiCl-KCl-$AlCl_3$-Er_2O_3 melts. J Rare Earths 31(2):192–197
36. Smolenski V, Novoselova A (2012) Electrochemistry of redox potential of the couple $Tm^{3+}Tm^{2+}$ and the formation of a Tm-Al alloy in fused NaCl-2CsCl eutectic. Electrochim Acta 63:179–184
37. Bermejo MR, Barrado E, Martínez AM, Castrillejo Y (2008) Electrodeposition of Lu on W and Al electrodes: electrochemical formation of Lu-Al alloys and oxoacidity reactions of Lu(III) in the eutectic LiCl-KCl. J Electroanal Chem 617:85–100
38. Yan YD, Yang XN, Huang Y, Xue Y, Zhang ML, Han W (2016) Direct electrochemical formation of different phases Al-Y alloys by codeposition in LiCl-KCl melts. Rare Metal Mat Eng 45:272–276
39. Li M, Liu YC, Han W, Wang SS, Zhang ML, Yan YD (2015) The electrochemical co-reduction of Mg-Al-Y alloys in the LiCl-NaCl-$MgCl_2$-AlF_3-YCl_3 melts. Metall Mater Trans B 46:644–652
40. Jang PN, Li HM, Kim WJ, Yun SC, Hwang GH (2019) Electrolytic preparation of Mg-Al-La alloys in KCl-$MgCl_2$-AlF_3 molten salts. J Mater Res Technol 8:5456–5463
41. Zhang JH, Wang J, Qiu X, Zhang DP, Tian Z, Niu XD, Tang DX, Meng J (2008) Effect of Nd on the microstructure, mechanical properties and corrosion behavior of die-cast Mg-4Al-based alloy. J Alloys Compd 464:556–564
42. Wang XQ, Li QN, Zhang XY (2008) Effects of yttrium and neodymium on microstructure and mechanical properties of AZ81 magnesium alloy. Rare Metal Mat Eng 37(1):62–65
43. Castrillejo Y, Bermejo MR, Barrado E, Martı´nez AM, Arocas PD, (2003) Solubilization of rare earth oxides in the eutectic LiCl-KCl mixture at 450 °C and in the equimolar $CaCl_2$/NaCl melt at 550 °C. J Electroanal Chem 545:141–157
44. Fukasawa K, Uehara A, Nagai T, Fujii T, Yamana H (2011) Electrochemical and spectrophotometric study on neodymium ions in molten alkali chloride mixtures. J Alloys Compd 509:5112–5118
45. Yamana H, Park BG, Shirai O, Fujii T, Uehara A, Moriyama H (2006) Electrochemically produced divalent neodymium in chloride melt. J Alloys Compd 408:66–70
46. Novoselova A, Smolenski V (2013) Electrochemical behavior of neodymium compounds in molten chlorides. Electrochim Acta 87:657–662
47. Tang H, Pesic B (2015) Electrochemistry and the mechanisms of nucleation and growth of neodymium during electroreduction from LiCl-KCl eutectic salts on Mo substrate. J Nucl Mater 458:37–44
48. Shen D, Akolkar R (2017) Electrodeposition of neodymium from $NdCl_3$-containing eutectic LiCl–KCl melts investigated using voltammetry and diffusion-reaction modeling. J Electrochem Soc 164(8):H5292–H5298
49. Liu K, Liu YL, Chai ZF, Shi WQ (2017) Evaluation of the electroextractions of Ce and Nd from LiCl-KCl molten salt using liquid Ga electrode. J Electrochem Soc 164(4):D169–D178
50. Sim JH, Kim YS, Paek SW, Kim SH, Lee SJ (2018) Electrode reactions of Nd^{3+}/Nd COUPLE in LiCl-KCl-$NdCl_3$ solutions at solid W and liquid Cd electrodes. Int J Electrochem Sci 13:2842–2859
51. Smolenski V, Novoselova A, Osipenko A, Caravaca C, Córdoba GD (2008) Electrochemistry of ytterbium (III) in molten alkali metal chlorides. Electrochim Acta 54:382–387
52. Masset P, Konings RJM, Malmbeck R, Serp J, Glatz JP (2005) Thermochemical properties of lanthanides (Ln = La, Nd) and actinides (An = U, Np, Pu, Am) in the molten LiCl-KCl eutectic. J Nucl Mater 344(1–3):173–197
53. Kim S, L SH, (2020) Electrochemical properties of $NdCl_3$ and $CeCl_3$ in molten LiCl-KCl eutectic salt. Appl Sci 10:7252–7262
54. Konishi H, Nishikiori T, Nohira T, Ito Y (2003) Thermodynamic properties of Dy/Ni intermetallic compounds. Electrochim Acta 48(10):1403–1408
55. Zhang ML, Yang YS, Han W, Li M, Ye K, Sun Y (2013) Electrodeposition of magnesium-lithium-dysprosium ternary alloys with controlled componen ts from dysprosium oxide assisted by magnesium chloride in molten chlorides. J Solid State Electrochem 17:2671–2678
56. Feng L, Guo C, Tang DX (1996) Relationship between the dissolution behaviours and current efficiencies of La, Ce, Pr and Nd in their chloride molten salts. J Alloys Compd 234(2):183–186
57. Akolkar R (2022) Perspective—is sustainable electrowinning of neodymium metal achievable? J Electrochem Soc 169:043501